Temporal hierarchy converges with spatial hierarchy: Intrinsic neural timescales follow core-periphery organization

Mehrshad Golesorkhi[1,2], Javier Gomez-Pilar[3,4], Shankar Tumati[2], Maia Fraser[5], Georg Northoff[2,6,7*]

1. School of Electrical Engineering and Computer Science, University of Ottawa, Ottawa, Canada
2. Mind, Brain Imaging and Neuroethics Research Unit, Institute of Mental Health, Royal Ottawa Mental Health Centre and University of Ottawa, Ottawa, Canada
3. Biomedical Engineering Group, University of Valladolid, Paseo de Belén, 15, 47011 Valladolid, Spain
4. Centro de Investigación Biomédica en Red en Bioingeniería, Biomateriales y Nanomedicina, (CIBER-BBN), Spain
5. Department of Mathematics and Statistics, University of Ottawa, Ottawa, Canada
6. Centre for Cognition and Brain Disorders, Hangzhou Normal University, Hangzhou, China
7. Mental Health Centre, Zhejiang University School of Medicine, Hangzhou, Zhejiang, China

Abstract

The human cortex exhibits a temporal hierarchy during task states as evidenced by intrinsic neural timescale. How the task-based intrinsic neural timescale is shaped by resting state's spatial topography especially the recently established core-periphery hierarchy (with the default-mode network (DMN) at the core and sensory networks at the periphery) remains an open issue. Using MEG data from the Human Connectome Project (HCP), we investigated the intrinsic neural timescales by measuring the autocorrelation window in short (ACW-50) and, introducing a novel variant, long (ACW-0) windows in various networks following core-periphery hierarchy. We demonstrate longer ACW-50 and ACW-0 in networks located at the core, i.e., DMN, frontoparietal network, and cingulum-operculum network, during both rest and task states. While networks at the periphery, i.e., auditory, visual, and somatomotor networks, exhibit shorter ACW-50 and ACW-0. Comparing both ACW scales during rest and task, i.e., rest-task difference revealed task- and network-specific effects. That is complemented by strong correlation of both ACW scales in rest with their counterpart during task states, following again the core-periphery hierarchy. Finally, we demonstrate that the longer window (ACW-0) exhibits better prediction in classifying a region's time window as belonging to either core or periphery. Overall, our findings provide fundamental insight into how the human cortex's temporal hierarchy of intrinsic neural timescales converges with spatial topography, the core-periphery hierarchy.

Introduction

Converging evidence shows an intrinsic temporal architecture in the brain [1,2,11–15,3–10]. Lower-order sensory and higher-order cognitive regions/networks exhibit different temporal features during task states, that is, "temporal receptive fields" [13] or "temporal receptive windows" [1,2,12,15–21,3–9,11]. Specifically, short segments like single words are processed mainly in lower-order regions like visual or auditory cortex while longer segments integrating different stimuli are processed in higher-order regions like default-mode network (DMN) and frontoparietal network (FPN) [1,2,12,15,16,19–22,3–9,11].

Analogously, hierarchical organisation has also been observed on the spatial side. Converging evidence shows micro- and macro-scale hierarchical organization in the human cortex following what has been described as 'core-periphery' [8,9,23–28]. A core-periphery (CP) architecture [29] can be characterized by a core that shares nodes with strong interconnections among each other; core-core connections ('dynamic core' or 'rich club'; [30–33] can be observed among regions included in the default-mode network (DMN), fronto-parietal network (FPN), and cingulum-operculum network (CON) [8,9,23–25,28]. These networks constituting the core have been distinguished from those at the opposite end of the core-periphery gradient; that is, visual, auditory, and somatomotor networks [8,9,23–25,28].

The observation of hierarchies in both temporal and spatial domains raises the question for their relationship. Specifically, one wants to investigate whether the different durations of the intrinsic neural timescales follow the spatial pattern of the core-periphery organisation. Is there potential convergence between spatial and temporal hierarchies holding across rest and task states? This is the main goal of our study.

Aims and hypotheses

The general aim of our study is to unravel whether the temporal hierarchy of intrinsic neural timescales follows in their regional distribution the spatial core-periphery (CP) hierarchy. For that purpose, we investigate MEG using rest and task data from the Human Connectome Project's (HCP) data set (see method for details). Specifically, we investigated the intrinsic neural timescales by measuring the autocorrelation function. Two window lengths were used – first, as per the standard method, ACW-50 was defined as the length of time where the person correlation was half-maximum, and second, a novel variant, ACW-0 was defined as the length of time at the first instance where the Pearson correlation reaches zero (See below for testing the differences between the two measures). The ACW-0 allows for measuring longer time windows, which are known to predominate in regions/networks like DMN at the core during task states [3–6]. Our overall hypothesis was that the temporal hierarchy of intrinsic neural timescales follows the spatial core-periphery with longer intrinsic neural timescales in networks at the core and shorter in periphery networks (see Fig. 1 for general overview of analyses as well as the main findings).

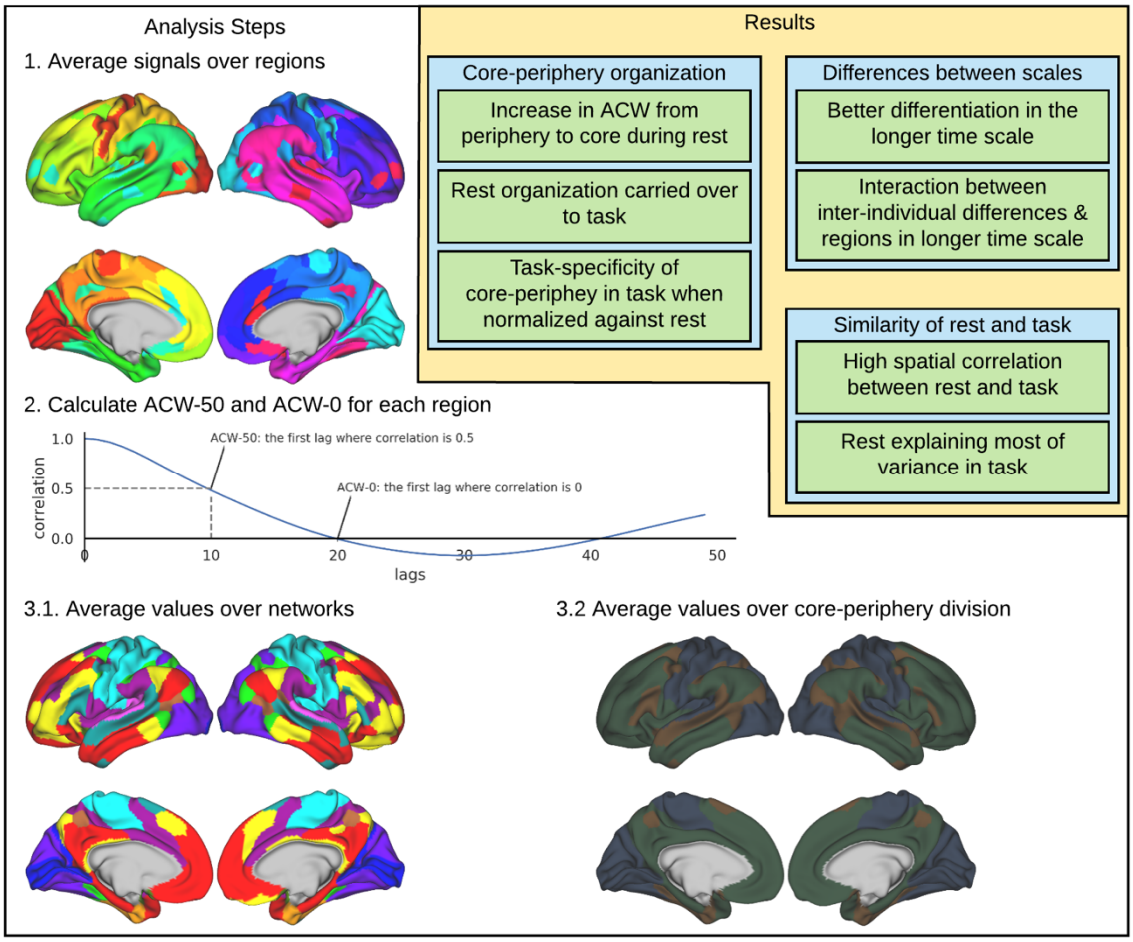

Figure 1. Schema of the paper. Represents the primary analysis conducted in this study. First, the time-series were averaged over 360 cortical brain regions provided by [34]. Then, ACF was calculated for each region and from that ACW-50 and ACW-0 were extracted. The ACW values were averaged over the 12 networks and along the core-periphery division for further analyses. The yellow box shows the results divided into three parts: core-periphery, scale differences and rest-task similarities.

The first specific aim was to investigate the intrinsic neural timescales in both resting and task states in those networks belonging to the core and the ones of the periphery (with one group of intermediate networks) [23,24]. Given converging neuro-anatomical findings in both core-periphery [24,26,28] and intrinsic neural timescales during task states [3–6], we hypothesized that networks belonging to the core, i.e., DMN, FPN, and CON, would show longer intrinsic neural timescales, i.e., ACW-50 and ACW-0, than those at the periphery, i.e., sensory and somatomotor network. Extending the findings of task-related 'temporal receptive windows' [3], we hypothesized that such correspondence of spatial and temporal core-periphery hierarchy would be present in both resting and task states.

The second specific aim consisted in investigating task-related effects of intrinsic neural timescales. For that purpose, we tested rest to task (rest-task) differences in ACW-50 and ACW-0. We expected task-related changes in our three different tasks. We also probed the impact of both region (as belonging to core or periphery) and subject (inter-individual differences) on short (ACW-50) and longer (ACW-0) timescales; for that we calculated probability density function in various ways (see results for details). Based on previous findings during task states [5,35], we expected high degrees of inter-individual differences in core regions like the DMN as well as, more generally, in those regions with longer temporal receptive windows.

Finally, our third aim was to directly link rest and task intrinsic neural timescales in both spatial and temporal terms. Given the known data about the carry-over of rest functional connectivity pattern to task states [36–38], we hypothesized analogous carry-over of the intrinsic neural timescale, i.e., ACW-50 and ACW-0, from rest to task resulting in high rest-task correlation. Moreover, as the spatial core-periphery hierarchy is already present at rest [23], we did not expect any difference in rest-task correlation between core and periphery networks. In contrast, given the differential relevance of long and short timescales in task states [3–5], we expected that ACW-50 and ACW-0 exhibit different classification probability of being associated with either regions in the core or regions associated with the periphery; this was tested for by machine learning and simulation.

Results

In this paper, our main aim was to investigate whether neural timescales conform to core-periphery (CP) architecture and how they'll be affected in task states. The primary analysis steps are illustrated in Fig. 1 and the findings are presented in the yellow box of the same figure.

ACW during resting state

In the first analysis, we calculated ACW values for each cortical region based on a template provided by [34] in resting state data. For each region, two ACW scales were calculated, i.e. ACW-50 and ACW-0 as the first lags where autocorrelation function (ACF) reaches correlation values of 0.5 and 0.0, respectively. ACW-50 and ACW-0 values were plotted over the brain regions to explore their spatial distribution (Fig. 2A left and B left, respectively).

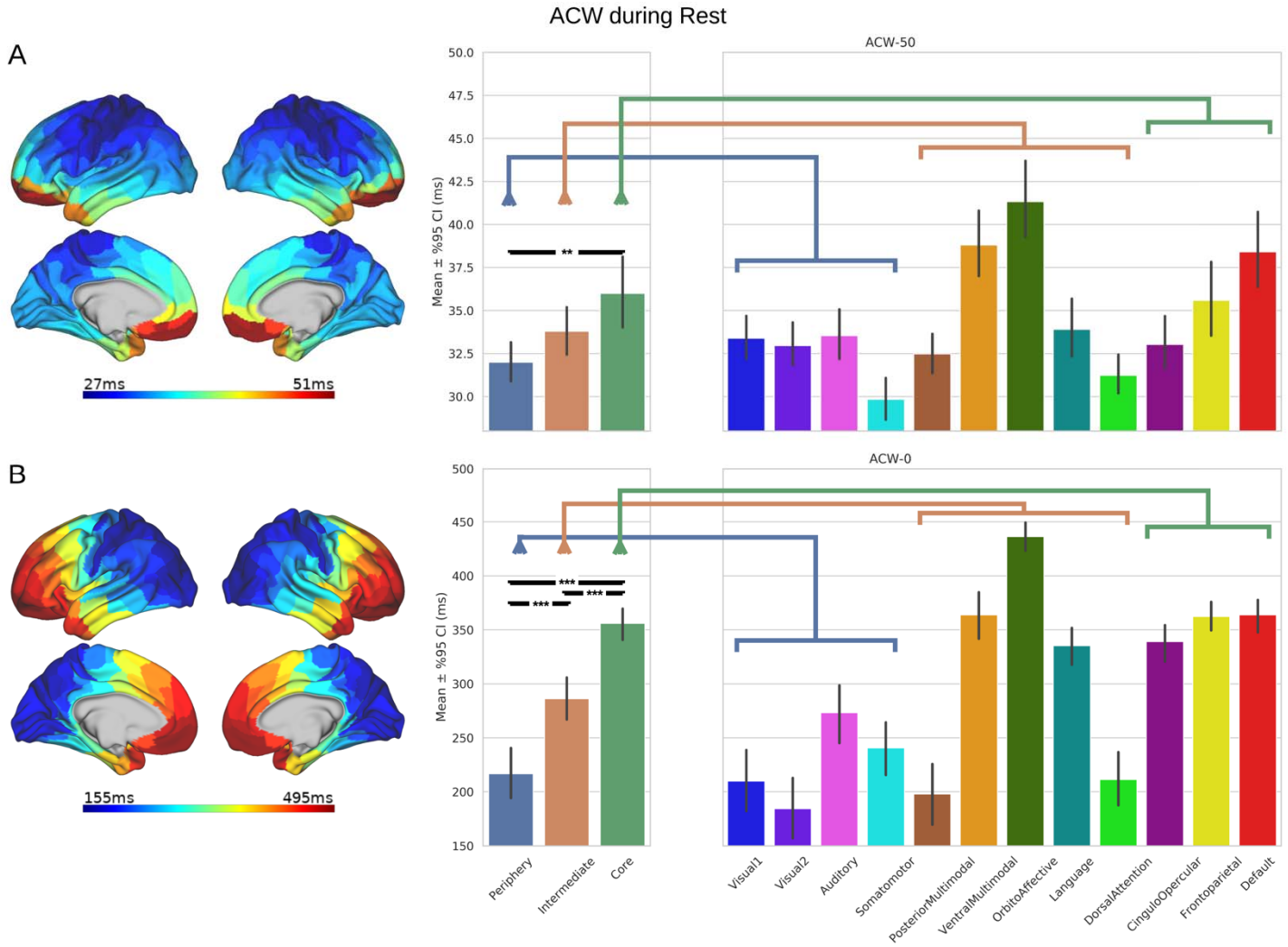

Figure 2. ACW during rest state. Each bar is average over subjects ± %95 confidence interval. Values are presented in milliseconds. A) Showing spatial distribution of ACW-50 over the brain cortical regions (left), averaged along CP division (middle) and over the 12 networks (right). The one-way Kruskal–Wallis test showed significant difference of ACW-50 for CP division ( ) and among the networks ( ). Post hoc analysis using Dunn's test showed significant difference between core and periphery in ACW-50 ( ). B) The same analysis as (A) for ACW-0. Left illustrates the ACW-0 over the brain regions, middle along the CP division and right is its values for each network. One-way Kruskal–Wallis was significant for difference of ACW-0 on CP division ( ) and among networks (

$0.001,\ df = 11$*). Post hoc analysis showed significant differences between all combinations of CP division (*$p < 0.001$*). In both ACW scales an increase in the values from periphery to core can be observed. Stars represent significance level (*$*** \equiv\ \alpha = 0.001, ** \equiv\ \alpha = 0.01, * \equiv\ \alpha = 0.05$*).*

Next, each region was designed to lie in either core or periphery by assigning a core-periphery (CP) label based on the network it was located in. Following [23], the regions in sensory networks (i.e. visual1, visual2, auditory and somatomotor) were assigned to periphery division (P), the ones in higher-order networks (i.e. cingular opercular, frontoparietal, and Default) to core division (C) and the remaining regions (i.e. regions in multimodal, orbito-affective, language and attention networks) to intermediate (I) division. The CP division (Fig. 2 middle, A for ACW-50 and B for ACW-0) shows an increase in both ACW scales from the periphery to the core. The difference between the three divisions was tested using Kruskal–Wallis one-way analysis of variance which showed significant differences between the three divisions, i.e., core, periphery, and intermediate (ACW-50: $\chi^2 = 11.2,\ \varepsilon^2 = 0.04,\ p = 0.003$, ACW-0: $\chi^2 = 71.8,\ \varepsilon^2 = 0.27;\ p < 0.001,\ df = 2$). Post hoc analysis using the Dunn's method showed significant difference between core and periphery in ACW-50 ($p < 0.01$) and all three combinations (i.e. core vs. periphery, core vs. intermediate and intermediate vs. periphery) in ACW-0 ($p < 0.001$).

The topography of ACW during resting state was further explored on a network level by averaging the values over regions in each one of the 12 networks. Plotting these values (Fig. 2A for ACW-50, Fig. 2B for ACW-0) revealed different spatial patterns among the networks. Again, using a non-parametric test, the differences were statistically significant (ACW-50: $\chi^2 = 175.8,\ \varepsilon^2 = 0.16$, ACW-0: $\chi^2 = 408.3,\ \varepsilon^2 = 0.38;\ p < 0.001,\ df = 11$).

ACW during task states

Task effect: To investigate the effect of task on ACW scales, we calculated ACW-50 and ACW-0 for the three different task conditions of StoryM, Motort and Wrkmem. The CP division revealed an increase in both ACW scales from periphery to core in all task conditions (Fig. 3 left, A for ACW-50 and B for ACW-0). Statistical differences followed along the CP division; non-parametric Kruskal-Wallis test (for each task) showed significant ($p < 0.001$) differences for both ACW-50 (StoryM: $\chi^2 = 61.4,\ \varepsilon^2 = 0.25$, Motort: $\chi^2 = 15.7,\ \varepsilon^2 = 0.08$, Wrkmem: $\chi^2 = 12.7,\ \varepsilon^2 = 0.05; df = 2$) and ACW-0 (StoryM: $\chi^2 = 130.1,\ \varepsilon^2 = 0.53$, Motort: $\chi^2 = 42.07,\ \varepsilon^2 = 0.23$, Wrkmem: $\chi^2 = 28.98,\ \varepsilon^2 = 0.15; df = 2$). Post hoc analysis in ACW-50 showed significant differences in core vs. periphery and intermediate vs. periphery in all task conditions and in core vs. intermediate in StoryM condition. For ACW-0, all combinations of post hoc were significant ($p < 0.001$). Furthermore, the network level topography of ACW scales (Fig. 3 right, A for ACW-50 and B for ACW-0) was also significantly different (among the 12 networks) across the subject for both ACW-50 (StoryM: $\chi^2 = 321.2,\ \varepsilon^2 = 0.32$, Motort: $\chi^2 = 117.7,\ \varepsilon^2 = 0.16$, Wrkmem: $\chi^2 = 126.3,\ \varepsilon^2 = 0.12$) and ACW-0 (StoryM: $\chi^2 = 612.6,\ \varepsilon^2 = 0.62$, Motort: $\chi^2 = 228.9,\ \varepsilon^2 = 0.31$, Wrkmem: $\chi^2 = 218.4,\ \varepsilon^2 = 0.22$). The task state results aligned with our resting state results suggesting that the ACW in both 50 and 0 scales were higher in the core regions during all three tasks thus following a CP regime during task states.

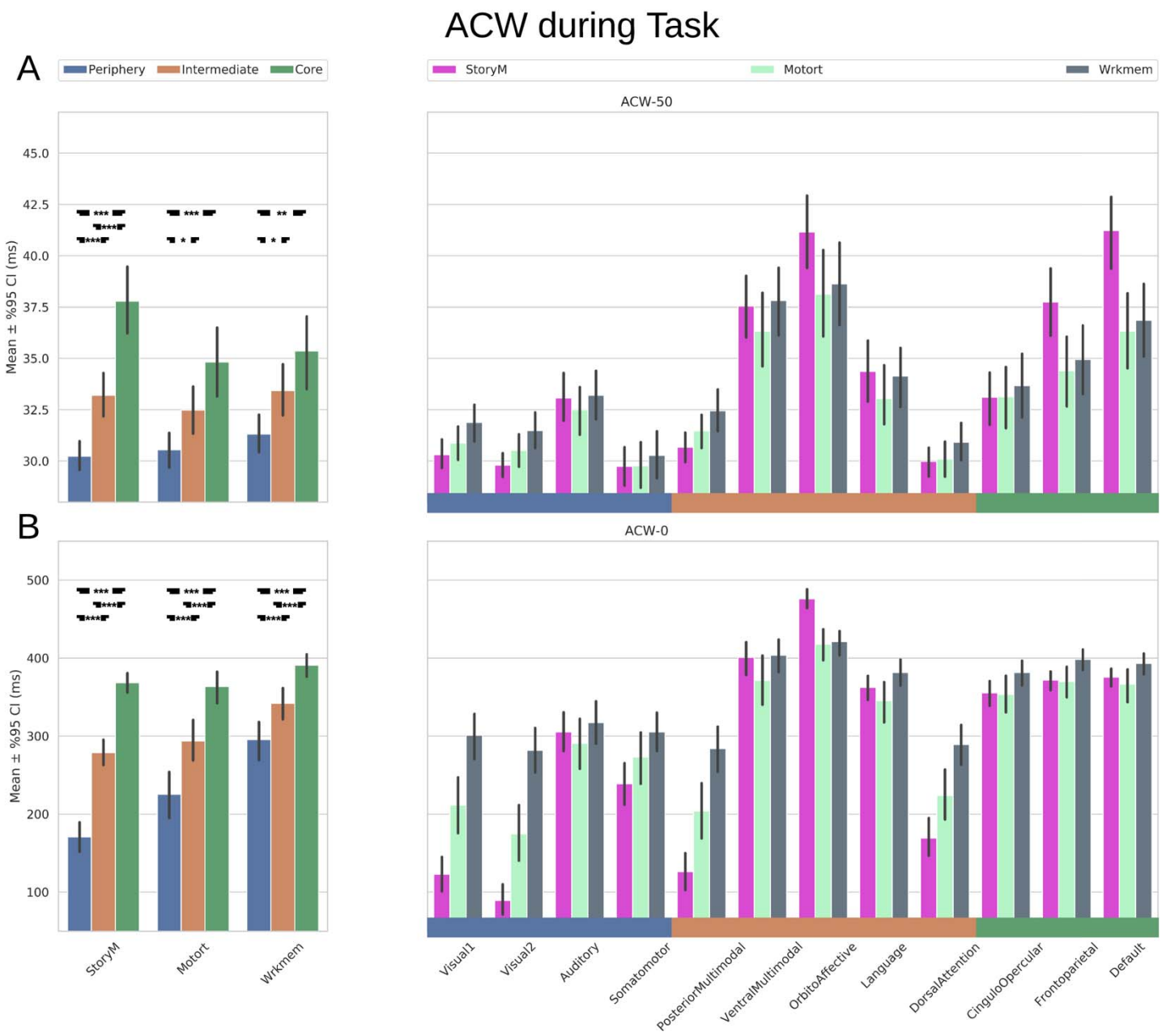

Figure 3. ACW during task state. Each bar is average over subjects ±%95 confidence interval. Values are presented in milliseconds. Brain spatial maps are provided in Fig. 6. A and B represent ACW-50 and ACW-0, respectively, along the CP division (left) and over different networks (right) for the three task conditions (StoryM, Motort, and Wrkmem). One-way Kruskal–Wallis (df for CP division = 2 and for networks = 11) showed significant ( ) differences along the CP division (StoryM: , Motort: , Wrkmem:) and among the networks (StoryM: , Motort: , Wrkmem:) in all three tasks for ACW-50 and along the CP division (StyoryM: , Motort: , Wrkmem:) and among networks (StoryM: , Motort: , Wrkmem:) for ACW-0. Similar to resting state results, increase in both ACW scales along the CP division can be observed in all task conditions. Post hoc analysis using Dunn's test revealed significant differences between core, periphery and intermediate divisions. Stars represent significance level ( ).

Degree of change from resting to task state: The next step was to investigate the degree of task-related changes relative to rest whether that change also conforms to a CP regime. For that, we calculated the percentage of

change (pchange) from resting to task states (see methods for details). Pchange was calculated per region and per subject in all three task conditions and was normalized against their respective resting state values, i.e., the degree of change from rest to task. The rest-task differences were investigated with respect to both CP division and networks themselves (independent of CP). Fig. 4 shows the result for both levels of both ACW scales.

Figure 4. Change in ACW from rest to task states. Each bar is the average percentage of change from rest state ±%95 confidence interval over subjects. Change in ACW-50 is showed in part A and ACW-0 in part B. Left plots show the change along the CP division and right among the networks. ACW-0 is associated with a consistent decrease from rest to task. The CP architecture observed in both resting and task state is broken to a task-specific structure when the effect of rest is removed from task.

We can see a prominent change in ACW-0 from rest to task. However, the direction of change is not similar among the three conditions (e.g. StoryM and Motort show opposite direction of change from rest in ACW-0); this holds for both ACW-50 and ACW-0. Together, these findings suggest task-specific effects in both

timescales, i.e., ACW-50 and ACW-0. Notably, the pattern of ACW-50 and ACW-0 rest-task changes no longer follows the CP division as it was observed during rest and task states separately.

The relationship between rest and task states in ACW

In this step, we investigated how the resting state's intrinsic neural timescales including their CP-gradient is carried over to task states; for that we conducted various analyses on rest-task similarity. The rest-task similarity analysis was performed in three steps, spatial correlation (calculation is illustrated in the box of Fig. 5), regional correlation (calculation is illustrated in the box of Fig. 6) and linear regression. The spatial correlation was used to see how similar the spatial distribution of ACW values are between all conditions (rest and task) (Fig. 6A for ACW-50 and B for ACW-0). We conducted spatial correlation between all pairs of conditions (e.g. Rest vs. StoryM or StoryM vs. Motort). Pearson correlation showed that the spatial distribution of both ACW measurements is highly correlated among all conditions (Rest, StoryM, Motort and Wrkmem) suggesting similar spatial topography of ACW in both scales (i.e. 50 and 0).

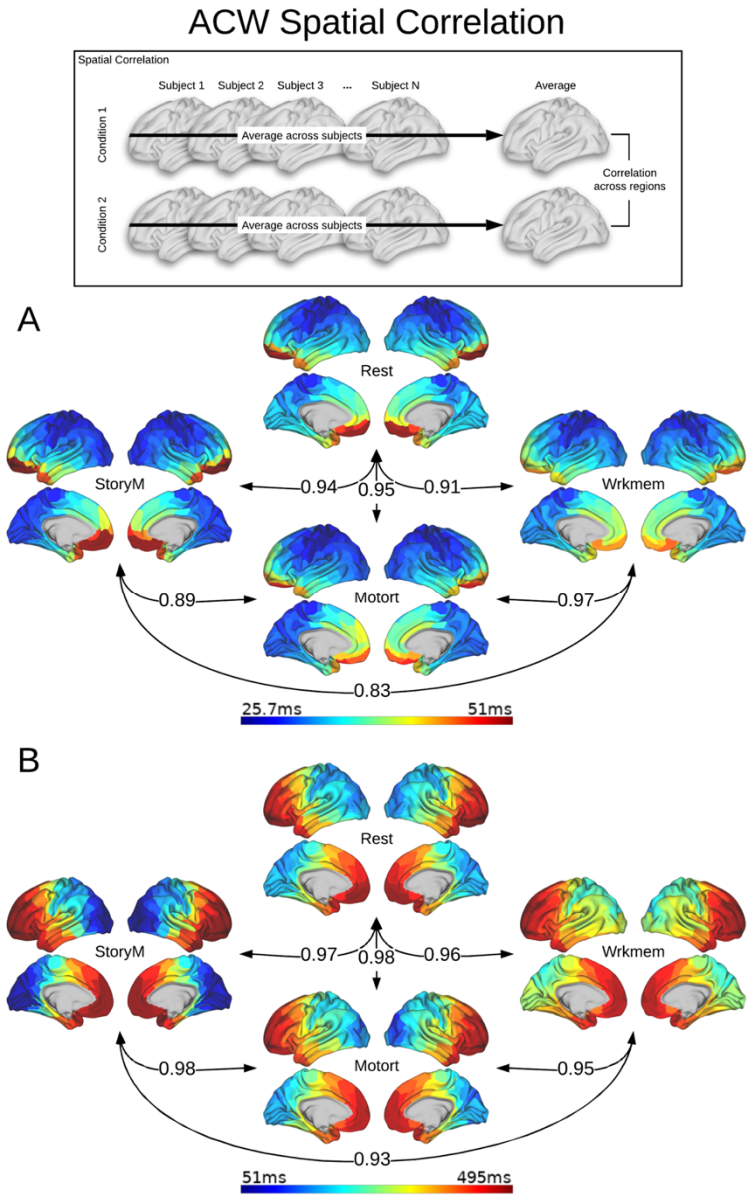

Figure 5. Spatial correlation among conditions. The box shows how spatial correlation is calculated. A and B show spatial correlation between different conditions alongside their individual spatial distribution over brain regions for ACW-50 and ACW-0, respectively. Each value on the arrows is a Pearson correlation coefficient between a pair of

conditions across the brain regions. All correlation values suggest that different conditions are highly correlated with each other.

Next, the rest-task similarity was further explored using regional correlation. The results were analogous for both ACW-50 (Fig. 6A top) and ACW-0 (Fig. 6A bottom). In both cases, first, Pearson correlation coefficient was calculated for each region over different subjects between Rest and all three task conditions (e.g. Rest vs. StoryM). Lastly, a single value per region (averaged over subjects) was calculated in all three task conditions and these values were used in separated linear regression models (a model per task condition) in which the task ACW was regressed as a function of rest ACW (Fig. 6B top for ACW-50 and bottom for ACW-0). The regression analysis revealed significant ($p < 0.001$) linear relationship between Rest and all three task conditions in ACW-50 (StoryM: R^2=0.87, Motort: R^2=0.89, Wrkmem: R^2=0.86) and ACW-0 (StoryM: R^2=0.94, Motort: R^2=0.96, Wrkmem: R^2=0.92) suggesting that rest ACW can explain more than 86% percent of the variance in task ACW. Together, the findings show strong rest-task similarity suggesting that the temporal and spatial hierarchy during the resting state is carried over to task states without showing task-specific effects.

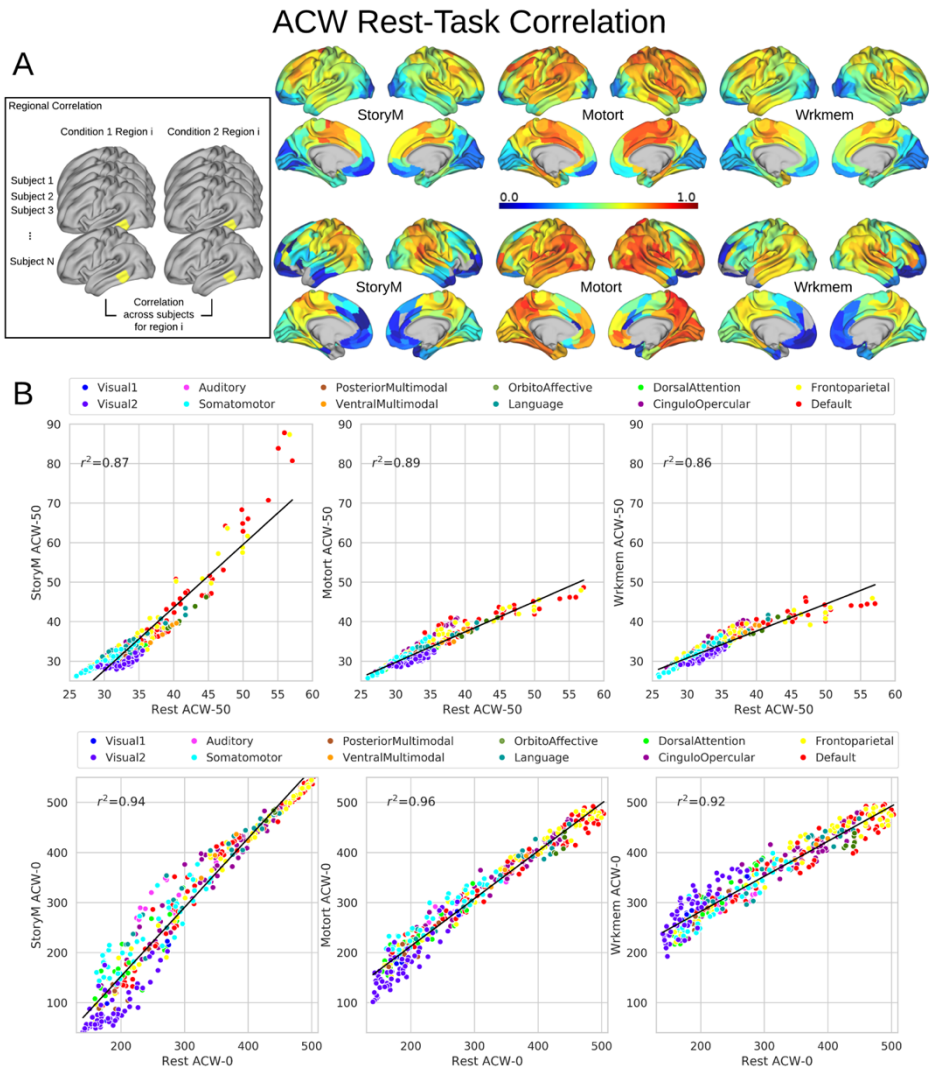

Figure 6. Rest-task relationship for ACW values through regional correlation and linear regression. The box represents how the regional correlation is calculated. A) Regional correlation between rest state and each task condition (top ACW-50 and bottom ACW-0). Correlation coefficients were calculated for each region over different subjects. B) Scatter plot of rest-task relationship over brain regions. Each dot represents a region's ACW-50 value averaged over subjects. The linear relationship in all conditions are significant at $\alpha = 0.001$ and they indicate that at least %86 variance of task is explained by rest.

The relationship between different timescales and their predictive power

Next, we investigated the relationship of ACW-50 and ACW-0 using four methods: kernel density estimation, simulation analysis, classification power, and inter-subject correlation.

First, a density estimation of the data was performed to observe the general density function (DF) over the whole data. We removed all the labels (e.g. task, subject, region) from our ACW values; then each ACW scale (i.e. 50 or 0) was normalized between 0 and 1. Based on the histograms of the data, we decided to use the Gaussian kernel with the expectation-maximization algorithm to estimate the two DFs (for ACW-50 and ACW-0). Fig. 7A (top left ACW-50, top right ACW-0) shows both histogram and the estimated DFs on them. It can be observed that the range of ACW-0 values is much wider than ACW-50; this suggests a better variety of ACW-0 values in the probability space which may allow for better differentiation between different labels (i.e., condition, subject, or region).

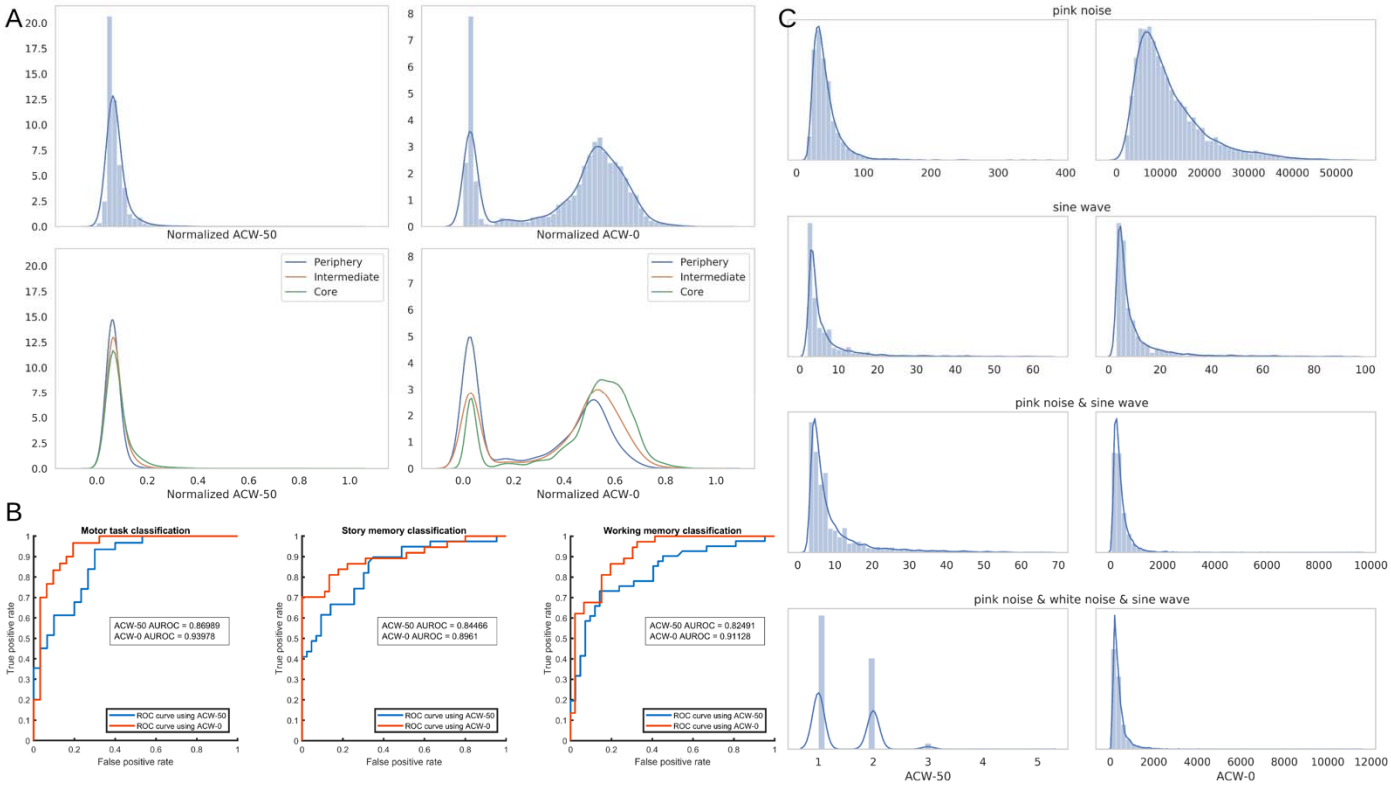

Figure 7. Relationship between ACW scales. A) Top: The density of the data removing all labels for condition, subject or region (left for ACW-50 and right for ACW-0). The data is normalized between 0 and 1 separately for ACW-50 and ACW-0. A) The density estimation suggests a single narrow Gaussian distribution for ACW-50 and two separate Gaussians for ACW-0. The double distribution of ACW-0 is only presented when the interaction of inter-individual differences with regional differences is taken into consideration. Moreover, ACW-0 is expanded over wider range of values compared to ACW-50 suggesting better differentiation capabilities. Bottom: The same data separated along the CP division. It suggests that low values of ACW-50 and ACW-0 lead to higher likelihood for a region to be in periphery category than core. However, it is the other way around for the second distribution in ACW-0 (located on larger ACW-0 values) suggesting higher likelihood for a region to be core than periphery. B) ROC curves for discriminating subjects in different tasks. They suggest that ACW-0 has better discriminative power among subjects than ACW-50. C) The density estimation of ACW values in simulated signals. Four categories of pink noise, sine wave, combination of pink noise and sine wave, and combination of pink and white noise with sine wave were used.

Importantly, the data suggest that ACW-0 follows two separate Gaussian distributions. To investigate whether these two distributions are related to subjects or/and regions, we repeated the same analysis several times each time averaging over one of the labels (e.g. averaging over regions to remove the regional differences, or, alternatively, averaging over subjects to remove the inter-individual differences; see Supp. Fig. 1). This revealed that the two separate DFs only appear when we take the interaction of inter-individual and inter-regional differences (subject X region) into consideration. That observation was consistent in all rest and task conditions suggesting that some subjects' regional ACW follows the first DF and some subjects follow the second one. Together, these findings suggest considerable inter-subject variability in specifically the longer timescale, i.e., ACW-0, whereas inter-subject variability was rather minimal in the shorter timescale, i.e., ACW-50.

To test for the impact of inter-individual differences on ACW-50 and ACW-0, the area under the Receiver Operating Characteristic (ROC) curve was computed for each task and measure. After labeling each subject as 'high variability' or 'low variability' based on its median split during resting after averaging across regions, the ACW-50 values during each task was used to generate the ROC curve (again, after averaging across regions). The same procedure was carried out using ACW-0 both for the median split and for generating the ROC curves, providing independent classification assessment for each measure. Results are shown in Fig. 7B suggesting that ACW-0 has better discriminative power among subjects than ACW-50.

To test how the density estimation behaves with respect to the CP architecture, we investigated DF estimations for core and periphery regions. The whole dataset (without labels) for each ACW scale were divided along our CP division. Six PDFs were estimated for them (2 ACW scale X 3 CP division) and plotted in Fig. 7A (bottom left for ACW-50 and bottom right for ACW-0). Observing those PDFs suggest that, when both ACW scales are in their lower range (first PDF), the respective region is more likely to belong to the periphery, i.e., sensory networks. In contrast, if especially the longer timescale, i.e., ACW-0, shows a higher value, i.e., being longer in its duration, the respective region has a higher likelihood of belonging to the core division.

In the second analysis, we simulated random oscillatory and noise signals to test the relationship between ACW-50 and ACW-0 in different kinds of signals. Pink noise and sine wave were used as the basis of our pseudo-aleatory signals. The signals were simulated in the same frequency range and sampling rate as our original data (1.3-45 Hz) with uniformly distributed random weights. 20000 signals categorised in four distinct categories (5000 each) were used: pure pink noise, pure sine wave, combination of sine and pink noise, and combination of sine, pink and white noise. Random uniform coefficients were used to linearly combine signals in the third and fourth categories (see Supp. Fig. 2 for a sample signal in each category). Pink noise was utilized to simulate scale-freeness [39], sine wave for oscillation and white noise for pure randomness. Both ACW scales were calculated for the signals and plotted against each other in Supp. Fig. 2. Kernel density of each category was also calculated (Fig. 7C); however, none of the simulated signals yielded the specific distributions like the ones previously observed in the brain signal.

Classification was used in the third analysis to determine if there is a difference in predicting core-periphery organization between the two scales. To simplify the question without losing generality, we designed a two-class classification problem using logistic regression classifier to determine if a signal is from a core (class 1) or periphery (class 2) region. All the other labels were removed from the data (i.e. condition, subject, network, and region). Thus, each sample in the model had a 1-D feature vector containing either ACW-50 or ACW-0 value and a label (whether core or periphery). In order to increase the reliability of the results, we used k-fold cross validation method with 20 folds. Table 1 summaries the results which show that not only the two scales have different performances, but also ACW-0 is a better predictor than ACW-50. The results were also replicated with support vector machine (SVM) classifier using radial basis function (RBF) kernel (Table 1). Next, we used univariate feature selection methods to determine which feature (ACW-50 or ACW-0) is better if we were required to choose one of the two. These methods work by selecting the best features based on univariate

statistical tests. We used mutual information, χ^2 test, false discovery rate, false positive rate, family wise error, and F-test (all implemented in scikit-learn library) and all of them consistently suggested ACW-0 as a better feature compared to ACW-50 when predicting a region's core or periphery association.

Table 1. The results for the 2-class classification problem. The values are averaged over 20 folds of K-fold cross validation algorithm using Logistic regression classifier. The results are presented if each sample has two features (both ACW-50 and ACW-0), or only one feature (either ACW-50 or ACW-0). They suggest better classification power for ACW-0 compared to ACW-50.

Algorithm	Model #	Features	Mean Accuracy (%)	Mean Precision (%)	Mean Recall (%)	Mean AUC of ROC
Logistic Regression	1	ACW-50 & ACW-0	69.14	63.33	46.61	74.12
	2	Only ACW-50	60.55	40.61	6.02	61.10
	3	Only ACW-0	69.08	63.37	46.12	74.45
SVM	1	ACW-50 & ACW-0	69.15	63.14	47.20	73.19
	2	Only ACW-50	61.61	41.21	7.01	48.72
	3	Only ACW-0	69.13	63.12	47.07	70.68

Finally, in the fourth analysis the difference between the two scales (ACW-50, ACW-0) was also observed (Supp. Fig. 3) with inter-subject correlations (ISC). Briefly, it was defined as the Pearson correlation coefficient between ACW value of the ith and j^{th} subjects over brain regions (more details in the method section). ISC can be interpreted as a measure of consistency across subjects. During resting state, the difference in ISC between core and periphery was larger for ACW-0 compared to ACW-50 (this was to some degree carried over to task states). These results further confirm that the interaction between ISC and core-periphery organization is different between ACW-50 and ACW-0 (Supp. Fig 3).

Discussion

The human cortex exhibits a temporal hierarchy with an intrinsic neural timescale. We demonstrate how such a temporal hierarchy is related to spatial core-periphery hierarchy with the former following the latter. Our findings show that the temporal hierarchy of intrinsic neural timescale measured by shorter and longer ACW, i.e., ACW-50 and ACW-0 converges with the spatial core-periphery hierarchy. Core networks exhibit longer intrinsic timescale, i.e., ACW-50 and ACW-0, than those at the periphery, which holds across both rest and task states. Comparing rest and task, i.e., rest-task differences, revealed task-specific changes as well as a strong rest-task correlation of ACW-50/ACW-0 on both spatial and temporal grounds conforming to the core-periphery hierarchy. Finally, we demonstrate that the longer timescale measure, i.e., ACW-0, exhibits higher degree of inter-subject variability and higher accuracy in differentially classifying core vs periphery regions. Together, we demonstrate that the temporal hierarchy of (shorter and longer) intrinsic neural timescales converges with the spatial core-periphery of the human cortex.

Core-periphery organization – converging spatial and temporal hierarchies

The spatial core-periphery hierarchy of human cortex has been observed in resting state [23–25,28]. We extend these findings beyond the spatial domain by showing a corresponding temporal hierarchy of intrinsic neural timescale. Animal [15] and modelling [1,8,9] studies observed different intrinsic neural timescales in lower- and higher-order regions/networks of the brain. This leaves open whether the human brain exhibits an analogous temporal architecture. Extending the animal and modelling findings to the human cortex, we, in rest states, observed shorter durations in ACW-50 and especially ACW-0 in periphery regions/networks like sensory and motor networks. That was complemented by longer ACW (especially in ACW-0) durations in the core networks like DMN, cingulum operculum, and FPN.

Together, these findings strongly suggest an intrinsic, i.e., network-specific, temporal architecture with different intrinsic neural timescales following the spatial core-periphery hierarchy. One may consequently want to speak of an integrated temporospatial core-periphery hierarchy. Future investigation is needed to establish a more intimate link between temporal and spatial dimensions. For instance, one may raise the question of whether the functional connectivity among the regions of the core, i.e., core-core connectivity, is directly related to the longer intrinsic timescale in these regions. Moreover, one may question whether the low degree of core-periphery connectivity is related to the discrepancy in their respective intrinsic neural timescale.

An analogous temporal core-periphery hierarchy was observed during task states. Periphery networks showed shorter ACW while core networks exhibited longer ACW. These findings suggest that the temporal core-periphery hierarchy of rest is carried over to task state holding across different tasks. One may consequently assume that the temporospatial core-periphery hierarchy may be an intrinsic feature that holds across different states, i.e., rest and task, and tasks, i.e., task-independent. That converges well with the observation that spatial core-periphery hierarchy has also been observed during task states [26] which may then be interpreted as simple carry-over from the rest. This remains to be explored in future studies.

Finally, findings on intrinsic neural timescale show higher-order networks like the DMN display the longest temporal receptive windows (based on functional connectivity) during equally complex tasks, i.e., story or movie [3–6,16,40]. We replicated these findings in terms of ACW during task states and extend it to the rest where an analogous temporal hierarchy was observed. Moreover, when comparing rest and task ACW, we observed task-specific effects that no longer followed the core-periphery hierarchy but rather the nature of the task. Finally, we demonstrate that the probability density of ACW shows a propensity towards longer ACW-0 in specifically the core networks while it remains shorter in periphery networks. This suggests some network-specific effects of longer (ACW-0) and also shorter (ACW-50) intrinsic neural timescale.

Rest shapes task states –temporal integration

Given that a core-periphery organization of intrinsic neural timescales in both rest and task states was observed, we tested for their relationship. We observed a high degree of correlation in the spatial differences for rest ACW-50/ACW-0 with their corresponding values in the three task states as well as among the three task states. That was complemented by high degrees in the correlation of the levels of ACW rest with those during the three task states. Together, these findings strongly support the assumption of an intrinsic temporal architecture in the brain that is preserved across rest and task states thus shaping both.

Our data suggest an intimate relationship between the intrinsic neural timescales during rest and task. We assume that such intimate relationship consists of temporal integration. The ACW and, more generally, the intrinsic neural timescales allow for temporal integration of stimuli through their temporal summing and pooling [41]. The need for temporal integration is especially relevant in complex stimuli or tasks like the movie: complex sequences of stimuli need to be integrated here to apprehend their meaning. This requires a prolonged autocorrelation window in especially higher-order networks as it is suggested by our rest-task findings.

In addition to the temporal integration of the various stimuli within the task itself, the external task-related stimuli need to be temporally integrated with the spontaneous activity's ongoing internal stimuli as related to internal cognition like mind wandering [42] and bodily inputs [43,44]. Such temporal integration may be mediated by the changes in the ACW during the transition from rest to the task [43,45]. This remains speculative at this point though. We currently do not know whether, and if so how, the length of the autocorrelation window in lower- and higher-order networks is related to different degrees of temporal integration of external, and internal stimuli (see [41] for first steps in this direction).

Limitations

Several limitations need to be mentioned. We employed a novel measure of time window, the ACW-0. While our findings show rest and task differences of ACW-0 compared to the shorter ACW-50, future studies both imaging and modelling, may be necessary to further establish their differences. Yet another question in this respect is whether ACW-50 and ACW-0 mediate different cognitive processes as it is suggested by their association with different regions/networks in the spatial hierarchy, i.e., core and periphery. Finally, modelling studies will be needed to establish causal relation between rest and task temporo-spatial hierarchies. While employing different measures of rest-task similarity, we were unable to establish causal rest-task connection in temporo-spatial hierarchies.

Conclusion

We show the convergence of the brain's temporal hierarchy, i.e., its intrinsic neural timescales, with the spatial core-periphery hierarchy during both rest and task states. This suggests intrinsic temporospatial core-periphery hierarchy in the human cortex shaping its cognitive processing during the transition from rest to task in both task-unspecific and task-specific ways. Our findings speak to the deeply ingrained temporo-spatial organisation and its dynamics shaping the brain's neural activity which, as postulated, may be central for understanding mental features like self and consciousness [46,47]. Correspondingly, alterations in the intrinsic temporospatial hierarchy may lead to systemic disruption of cognitive function as it can typically be observed in psychiatric disorders like schizophrenia and depression.

Acknowledgments

This research has received funding from the European Union's Horizon 2020 Framework Program for Research and Innovation under the Specific Grant Agreement No. 785907 (Human Brain Project SGA2). GN is grateful for funding provided by UMRF, uOBMRI, CIHR and PSI. We are also grateful to Chris J. Honey for giving useful suggestions.

Materials and Methods

Experimental model and subject details. The analyses involved magnetoencephalography (MEG) data of 89 subjects from the Human Connectome Project (HCP) WU-Minn HCP 1200 subjects data release [48]. Rest state MEG data were acquired in runs of approximately 6 minutes. During the scan, the subjects were instructed to relax with eyes open and maintain fixation on a red crosshair. ECG and EOG recordings were also performed. Following the completion of resting state MEG, subjects were asked to complete three tasks of language processing (story vs. math, StoryM), motor (Motort) and working memory (Wrkmem). Task MEG data were acquired with the same parameters as the rest. Each task was approximately 7, 14 and 10 for StoryM, Motort and Wrkmem, respectively. The sampling frequency was 2034.5 Hz.

Task paradigms. The tasks were all block-design paradigms. In the working memory task, participants were instructed to retain images in their visual working memory and compare them with subsequently presented images. The language processing task consisted of 7 blocks of a story task interleaved with 15 blocks of a math task. The story blocks presented participants with brief auditory stories. Motor processing was assessed using a task in which participants were presented with visual cues instructing the movement of either the right hand, left hand, right foot, or left foot. The paradigm of each task is extensively discussed in the WU-Minn HCP 1200 Subjects data release manual.

Preprocessing. The HCP released preprocessed data. It included the following steps: removal of artifacts, bad channels, and bad segments based on HCP quality assurance standards [49], bandpass (1.3–150 Hz) and notch (59–61 Hz, 119–121 Hz) filtering, and removal of non-brain components through ICA.

Source reconstruction was conducted similar to a recent article by [18], which used the same HCP data. Briefly, reconstruction was done for 8004 vertices (8k space) on the cortical surface using Fieldtrip and software provided by HCP. First, we applied a low-pass filter (45 Hz) on the sensor data, which was projected on to source space by synthetic aperture magnetometry. The details of the projection are provided in [18]. After source reconstruction, time courses were parcellated using the 360 cortical areas provided by [34]. The template was resampled to 8K space using resampling tools available in the HCP workbench software. Finally, the time courses were averaged over runs resulting in four conditions of Rest (resting state MEG), StoryM, Motort, and Wrkmem (task states MEG).

Calculation of the metrics. In the next step, autocorrelation (ACF) of the regions' time courses were calculated within the statsmodel library [50] using the fast Fourier transform algorithm. From that, two ACW values were extracted per autocorrelation function: the first lag (in milliseconds) where the autocorrelation decays to 50% of its maximum (ACW-50) and the first instance where the lag reaches zero (ACW-0).

Network construction. The ACW values were further averaged into cortical networks (per subject) based on the recent template provided by [34]. The template includes 12 cortical networks - visual1, visual2, auditory, somatomotor, posterior multimodal, ventral multimodal, orbitoaffective, language, dorsal attention, cinguloopercular, frontoparietal, and default-mode.

Core-periphery division. To analyze the core-periphery (CP) hypothesis, the regional data was divided into three categories of periphery, intermediate and core base on where in the brain they were located. Regions belonging to visual1, visual2, auditory, and somatomotor networks were placed into periphery division (P). Similar to that, regions in cinguloopercular, frontoparietal and default networks were placed into the core division (C). Finally, the remaining regions (which belonged to the other five networks) were categorized as intermediate (I).

Spatial correlation was used to measure the spatial similarity between different conditions. It was calculated as a single Pearson's ρ correlation coefficient for a pair of conditions (e.g. Rest vs. StoryM) over brain regions after averaging over subjects (thus creating a single brain per condition, illustrated in the box of Fig. 6).

Regional correlation was used to measure the regional similarity between different conditions. This correlation was calculated for each region across subjects between a pair of conditions (illustrated in the box of Fig. 7).

Percentage change from rest. The difference between rest and task state was calculated as a percentage of change per region per subject. Each region's rest and task (e.g. StoryM) values were put in the $\frac{REST - TASK}{REST} \times 100$ formula to both measure the change from the rest to the task and normalize against the rest at the same time.

Linear regression was performed to investigate the relationship between resting state and task state. The regional values were averaged over subjects and then put into the regression model.

Density estimation. To observe the individuality and regionality effects of ACW scales we estimated the probability distribution of the data, removing all the labels. It means that for each scale (whether 50 or 0) all the data from all tasks, regions, and subjects were put together and fed to the estimation algorithm. Estimation was performed using the statsmodel's kernel density estimator (KDEUnivariate).

ROC curves. The area under the Receiver Operating Characteristic (ROC) curve was used to show the relationship between inter-individual differences and ACW scales. ROC is a well-known metric for diagnostic test evaluation. In a ROC curve the true positive rate is plotted as a function of the false positive rate for different cut-off points of a parameter (ACW-50 or ACW-0). The area under the ROC curve (AUC) is a measure of how well the parameter can distinguish between two diagnostic groups (low variability subjects compared to high variability ones.

Classification using logistic regression. In order to investigate the discriminative power of the two ACW scales, a 2-class classification problem was used with the logistic function as the classifier. Each region's signal was labeled either core (class 1) or periphery (class 2). Then, for each region the ACW values were used as features. Three different models were created. Model 1 used both ACW values as features (each sample had two features), Model 2 used only ACW-50 and the third model used only ACW-0. The training and testing were conducted using K-fold cross validation algorithm with 20 folds. Accuracy, precision, recall, and the area under the AUC curve was calculated as efficiency metrics. All of the classification steps were implemented using the scikit-learn library of Python programming language.

Feature selection. To select one of the two features (ACW-50 or ACW-0) as the better one, a set of univariate feature selection algorithms were used. These methods work by selecting the best features based on univariate statistical tests. SelectKBest, SelectPercentile, SelectFpr, SelectFdr, and SelectFwe methods, implemented in scikit-learn library, using both mutual information and χ^2 test as metrics were used. Please refer to https://scikit-learn.org/stable/modules/feature_selection.html#univariate-feature-selection for detailed explanation of each method.

Inter-subject correlation. As a confirmatory analysis, inter-subject correlation (ISC) was calculated for each condition (either rest or task) separating for core and periphery regions. ISC is a matrix of correlation coefficient values. The cell at index ij of the ISC matrix is the Pearson correlation coefficient between subjects i and j across regions. A total of 16 ISC matrices were calculated, each a combination of a condition (Rest, StoryM, Motort and StoryM), a CP category (core and periphery), and an ACW scale (50 and 0). An ISC can be considered as a measure of similarity among subjects.

Simulated Signals. The relationship between ACW-50 and ACW-0 was investigated using simulation analysis. 20000 pseudo-aleatory signals within four different categories (5000 each) were simulated. Autocorrelation function of each signal was calculated and from that ACW scales were extracted. The categories included (I) pink noise, (II) sine wave, and linear combinations of (III) pink noise and sine wave, and (IV) pink noise, white noise and sine wave. Uniformly distributed random weights were used for the linear combinations and the frequency of the sine waves. The frequency range and sampling rate was fixed to be equal to our real data. Pink noise was chosen to model the scale-free behavior (58), white noise for pure randomness and sine wave for oscillation. For each category two density functions were calculated (one for each ACW scale), and compared to the density functions of our real data.

Statistics. All statistical analyses were performed in the statsmodel library [50] and R v.3.6 and all p-values were corrected for multiple comparison using the Benjamini-Hochberg Procedure. Kruskal–Wallis one-way analysis of variance was with either twelve factors for the network analysis or three factors for the PC division analysis was performed. For significant results, post hoc analysis using the Dunn's test was conducted to show the within factor differences.

Software. All steps of the data processing were performed with in-house scripts written in Python programming language using NumPy, SciPy, cifti, joblib, matplotlib, and seaborn libraries. The source code is freely available at www.georgnorthoff.com/codes/. For brain map visualization purposes, wb_view (part of Connectome Workbench software, https://www.humanconnectome.org/software/connectome-workbench) was used.

References

1. Chaudhuri, R., Knoblauch, K., Gariel, M. A., Kennedy, H. & Wang, X. J. A Large-Scale Circuit Mechanism for Hierarchical Dynamical Processing in the Primate Cortex. *Neuron* **88**, 419–431 (2015).
2. Chaudhuri, R., He, B. J. & Wang, X. J. Random recurrent networks near criticality capture the broadband power distribution of human ECoG dynamics. *Cereb. Cortex* **28**, 3610–3622 (2018).
3. Hasson, U., Chen, J. & Honey, C. J. Hierarchical process memory: Memory as an integral component of information processing. *Trends Cogn. Sci.* **19**, 304–313 (2015).
4. Chen, J., Hasson, U. & Honey, C. J. Processing Timescales as an Organizing Principle for Primate Cortex. *Neuron* (2015) doi:10.1016/j.neuron.2015.10.010.
5. Chen, J. *et al.* Shared memories reveal shared structure in neural activity across individuals. *Nat. Neurosci.* **20**, 115–125 (2017).
6. Honey, C. J. *et al.* Slow Cortical Dynamics and the Accumulation of Information over Long Timescales. *Neuron* **76**, 668 (2012).
7. Huang, Z., Liu, X., Mashour, G. A. & Hudetz, A. G. Timescales of intrinsic BOLD signal dynamics and functional connectivity in pharmacologic and neuropathologic states of unconsciousness. *J. Neurosci.* **38**, 2304–2317 (2018).
8. Gollo, L. L. *et al.* Dwelling quietly in the rich club: Brain network determinants of slow cortical fluctuations. *Philos. Trans. R. Soc. B Biol. Sci.* **370**, 20140165 (2015).
9. Gollo, L. L., Roberts, J. A. & Cocchi, L. Mapping how local perturbations influence systems-level brain dynamics. *Neuroimage* **160**, 97–112 (2017).
10. Raut, R. V. *et al.* Organization of Propagated Intrinsic Brain Activity in Individual Humans. *Cereb. Cortex* **30**, 1716–1734 (2020).
11. Kiebel, S. J., Daunizeau, J. & Friston, K. J. A hierarchy of time-scales and the brain. *PLoS Comput. Biol.* **4**, e1000209 (2008).
12. Bernacchia, A., Seo, H., Lee, D. & Wang, X. J. A reservoir of time constants for memory traces in cortical neurons. *Nat. Neurosci.* (2011) doi:10.1038/nn.2752.
13. Cavanagh, S. E., Wallis, J. D., Kennerley, S. W. & Hunt, L. T. Autocorrelation structure at rest predicts value correlates of single neurons during reward-guided choice. *Elife* (2016) doi:10.7554/eLife.18937.
14. Zilio, F. *et al. Intrinsic neural time scales are related to sensory rather than motor processing – Evidence from abnormal behavioral states.*
15. Murray, J. D. *et al.* A hierarchy of intrinsic timescales across primate cortex. *Nat. Neurosci.* **17**, 1661 (2014).
16. Stephens, G. J., Honey, C. J. & Hasson, U. A place for time: The spatiotemporal structure of neural dynamics during natural audition. *J. Neurophysiol.* (2013) doi:10.1152/jn.00268.2013.
17. Wolff, A. *et al.* The temporal signature of self: Temporal measures of resting-state EEG predict self-consciousness. *Hum. Brain Mapp.* **40**, 789–803 (2019).
18. Demirtaş, M. *et al.* Hierarchical Heterogeneity across Human Cortex Shapes Large-Scale Neural Dynamics. *Neuron* **101**, 1181-1194.e13 (2019).
19. Watanabe, T., Rees, G. & Masuda, N. Atypical intrinsic neural timescale in autism. *eLife* vol. 8 (2019).
20. Cocchi, L., Gollo, L. L., Zalesky, A. & Breakspear, M. Criticality in the brain: A synthesis of neurobiology, models and cognition. *Prog. Neurobiol.* **158**, 132–152 (2017).
21. Runyan, C. A., Piasini, E., Panzeri, S. & Harvey, C. D. Distinct timescales of population coding across cortex. *Nature* (2017) doi:10.1038/nature23020.
22. Baria, A. T. *et al.* Linking human brain local activity fluctuations to structural and functional network architectures. *Neuroimage* (2013) doi:10.1016/j.neuroimage.2013.01.072.
23. Margulies, D. S. *et al.* Situating the default-mode network along a principal gradient of macroscale cortical organization. *Proc. Natl. Acad. Sci. U. S. A.* **113**, 12574–12579 (2016).
24. Huntenburg, J. M., Bazin, P. L. & Margulies, D. S. Large-Scale Gradients in Human Cortical Organization. *Trends Cogn. Sci.* **22**, 21–31 (2018).

25. Wang, P. *et al.* Inversion of a large-scale circuit model reveals a cortical hierarchy in the dynamic resting human brain. *Trop. Subtrop. Agroecosystems* **21**, (2019).
26. Murphy, C. *et al.* Distant from input: Evidence of regions within the default mode network supporting perceptually-decoupled and conceptually-guided cognition. *Neuroimage* **171**, 393–401 (2018).
27. Bassett, D. S. *et al.* Hierarchical organization of human cortical networks in health and Schizophrenia. *J. Neurosci.* (2008) doi:10.1523/JNEUROSCI.1929-08.2008.
28. Huntenburg, J. M. *et al.* A Systematic Relationship Between Functional Connectivity and Intracortical Myelin in the Human Cerebral Cortex. *Cereb. Cortex* (2017) doi:10.1093/cercor/bhx030.
29. Borgatti, S. P. & Everett, M. G. Models of core/periphery structures. *Soc. Networks* (2000) doi:10.1016/S0378-8733(99)00019-2.
30. van den Heuvel, M. P. & Sporns, O. Network hubs in the human brain. *Trends Cogn. Sci.* **17**, 683–696 (2013).
31. Tononi, G. & Edelman, G. M. Consciousness and complexity. *Science* (1998) doi:10.1126/science.282.5395.1846.
32. de Pasquale, F. *et al.* A Cortical Core for Dynamic Integration of Functional Networks in the Resting Human Brain. *Neuron* **74**, 753–764 (2012).
33. de Pasquale, F., Corbetta, M., Betti, V. & Della Penna, S. Cortical cores in network dynamics. *Neuroimage* **180**, 370–382 (2018).
34. Ji, J. L. *et al.* Mapping the human brain's cortical-subcortical functional network organization. *Neuroimage* **185**, 35–57 (2019).
35. Chen, J. *et al.* Accessing Real-Life Episodic Information from Minutes versus Hours Earlier Modulates Hippocampal and High-Order Cortical Dynamics. *Cereb. Cortex* **26**, 3428–3441 (2016).
36. Cole, M. W., Bassett, D. S., Power, J. D., Braver, T. S. & Petersen, S. E. Intrinsic and task-evoked network architectures of the human brain. *Neuron* (2014) doi:10.1016/j.neuron.2014.05.014.
37. Cole, M. W., Ito, T., Bassett, D. S. & Schultz, D. H. Activity flow over resting-state networks shapes cognitive task activations. *Nat. Neurosci.* (2016) doi:10.1038/nn.4406.
38. Cole, M. W. *et al.* Multi-task connectivity reveals flexible hubs for adaptive task control. *Nat. Neurosci.* **16**, 1348 (2013).
39. He, B. J., Zempel, J. M., Snyder, A. Z. & Raichle, M. E. The temporal structures and functional significance of scale-free brain activity. *Neuron* **66**, 353–369 (2010).
40. Lerner, Y., Honey, C. J., Silbert, L. J. & Hasson, U. Topographic mapping of a hierarchy of temporal receptive windows using a narrated story. *J. Neurosci.* **31**, 2906–2915 (2011).
41. Himberger, K. D., Chien, H. Y. & Honey, C. J. Principles of Temporal Processing Across the Cortical Hierarchy. *Neuroscience* vol. 389 161–174 (2018).
42. Christoff, K., Irving, Z. C., Fox, K. C. R. R., Spreng, R. N. & Andrews-Hanna, J. R. Mind-wandering as spontaneous thought: A dynamic framework. *Nat. Rev. Neurosci.* **17**, 718–731 (2016).
43. Northoff, G. *Unlocking the Brain*. *Unlocking the Brain* (2014). doi:10.1093/acprof:oso/9780199826995.001.0001.
44. Tallon-Baudry, C., Campana, F., Park, H.-D. & Babo-Rebelo, M. The neural monitoring of visceral inputs, rather than attention, accounts for first-person perspective in conscious vision. *Cortex* **102**, 139–149 (2018).
45. Northoff, G., Qin, P. & Nakao, T. Rest-stimulus interaction in the brain: a review. *Trends Neurosci.* **33**, 277–284 (2010).
46. Northoff, G. *The Spontaneous Brain*. *MIT Press* (2019). doi:10.7551/mitpress/11046.001.0001.
47. Northoff, G. & Tumati, S. "Average is good, extremes are bad" – Non-linear inverted U-shaped relationship between neural mechanisms and functionality of mental features. *Neuroscience and Biobehavioral Reviews* (2019) doi:10.1016/j.neubiorev.2019.06.030.
48. Van Essen, D. C. *et al.* The WU-Minn Human Connectome Project: An overview. *Neuroimage* **80**, 62–79 (2013).
49. Larson-Prior, L. J. *et al.* Adding dynamics to the Human Connectome Project with MEG. *Neuroimage*

(2013) doi:10.1016/j.neuroimage.2013.05.056.
50. Seabold, S. & Perktold, J. *Statsmodels: Econometric and Statistical Modeling with Python*. *PROC. OF THE 9th PYTHON IN SCIENCE CONF* (2010).